Front. Phys. 10, 100503 (2015)
DOI 10.1007/s11467-015-0462-4

RESEARCH ARTICLE

Optimal configuration for vibration frequencies in a ring of harmonic oscillators: The nonidentical mass effect

Shuai Liu[1], **Guo-Yong Zhang**[2,3], **Zhiwei He**[2,4], **Meng Zhan**[2,†]

[1] *College of Science, Northwest A&F University, Yangling 712100, China*

[2] *Wuhan Center for Magnetic Resonance, State Key Laboratory of Magnetic Resonance and Atomic and Molecular Physics, Wuhan Institute of Physics and Mathematics, Chinese Academy of Sciences, Wuhan 430071, China*

[3] *College of Computer Science and Technology, Hubei Normal University, Huangshi 435002, China*

[4] *University of the Chinese Academy of Sciences, Beijing 100049, China*

Corresponding author. E-mail: [†] *zhanmeng@wipm.ac.cn*

Received October 23, 2014; accepted December 29, 2014

The parameter diversity effect in coupled nonidentical elements has attracted persistent interest in nonlinear dynamics. Of fundamental importance is the so-called optimal configuration problem for how the spatial position of elements with different parameters precisely determines the dynamics of the whole system. In this work, we study the optimal configuration problem for the vibration spectra in the classical mass–spring model with a ring configuration, paying particular attention to how the configuration of different masses affects the second smallest vibration frequency (ω_2) and the largest one (ω_N). For the extreme values of ω_2 and ω_N, namely, $(\omega_2)_{\min}$, $(\omega_2)_{\max}$, $(\omega_N)_{\min}$, and $(\omega_N)_{\max}$, we find some explicit organization rules for the optimal configurations and some approximation rules when the explicit organization rules are not available. The different distributions of ω_2 and ω_N are compared. These findings are interesting and valuable for uncovering the underlying mechanism of the parameter diversity effect in more general cases.

Keywords synchronization, vibration frequencies, normal modes, complex systems

PACS numbers 05.45.Xt, 63.20.D-, 89.75.Fb

1 Introduction

In the past decades, the study of various dynamical processes of coupled nonlinear systems [1–14] became a well-studied topic, attracting a great deal of interest in diverse research areas including physics, chemistry, biology, sociology, and engineering technology. The rich dynamical behaviors of these processes include synchronization [15–23], splay states [24–26], amplitude death [27–29], self-organized criticality [30], consensus in multi-agent systems [31], and epidemic spreading [32], just to name a few. Uncovering the organizing rules for these distinct dynamical processes in coupled systems poses a great challenge.

Although most previous studies focused on systems of coupled *identical* elements, such as the complete (state) synchronization in coupled chaotic systems based on a stability analysis of synchronization in the framework of the master stability function (or eigenvalue analysis) [15–22], the assumption that the elements are identical is never practical in any realistic world, where the system elements always display a disparity in the values of some characteristic parameters. A distinguished case is the model of power grids [33–35], for which the system characteristic parameters for the identical nodal dynamics of the generators and users have to be chosen as positive and negative, respectively, owing to the supply–demand balance.

Therefore, it is quite natural that this problem of system parameter diversity has aroused continuous interest of researchers in nonlinear dynamics field, with some unusual effects of parameter diversity being discovered [36–51]. For instance, Braiman *et al.* found that, to our great surprise, the parameter diversity can be used to tame spatiotemporal chaos [36]. Later work on the disordered driving forces exerted on phases revealed the same result [38]. Some nontrivial effects of parameter diversity and the spatial independence of noise have been studied in the framework of array-enhanced coherence resonance [39]. Recently, a novel concept, diversity-induced resonance, has been proposed by Tessone and cowork-

ers, who found that the system's response subjected to an external subthreshold signal is optimized for an intermediate value of diversity, indicating a constructive role of intrinsic diversity [40]. This counterintuitive effect, diversity-induced resonance, has been extensively found in ensembles of coupled bistable or excitable systems [40] and in some other coupled systems [41, 42]. Despite these extensive *statistical* investigations on the parameter diversity effect, however, we are still at a very early stage of fully understanding the underlying mechanism for all these peculiar diversity-induced order effects.

To fill this gap, recently some of the authors and coworkers have proposed the *optimal configuration problem* [47–51] with the intention of ascertaining how the spatial position of elements with different parameters precisely determines the dynamics of the whole system. Basically, this is a difficult problem and fundamentally differs in manner from that of all previous studies on diversity, in which nonidentical parameters were usually randomly chosen from a fixed interval with a uniform or Gaussian distribution and only statistical effects were investigated; see, e.g., Refs. [36–40]. For instance, we studied the influences of different spatial frequency distributions on the efficiency of frequency synchronization and defined a physical quantity "roughness" R as a function of frequency configuration, which monotonically determines the efficiency of frequency synchronization [47]. Therefore, we found that synchronizing a sufficiently large number of nonidentical oscillators with a very small coupling is possible if we can properly reshuffle the spatial positions of nodes; this is essentially distinct from the common sense that full frequency synchronization in a system of infinitely large size typically requires an infinitely large coupling strength. Recently, we have generalized this optimal configuration problem to some other dynamical behaviors, such as the oscillation death in coupled nonidentical periodic or chaotic oscillators [49, 50] and vibration spectra in the classical mass–spring model with different masses on complex networks [51]. For sufficiently random networks, we found that the second smallest vibrational frequency ω_2 becomes maximal and the largest vibrational frequency ω_N becomes minimal if the node degrees are point-to-point-positively correlated with the masses [51]. Moreover, ω_2 becomes minimal under the condition that the heaviest mass is placed on the lowest-degree vertex, ω_N is maximal as long as the lightest mass is placed on the highest-degree vertex, and, in both cases, all other masses can be arbitrarily settled. These findings indicate that the matchings between the node parameter and the node position rule the global system dynamics, and sometimes only one node is enough to control the collective behaviors of the whole system.

In the classical mass–spring model [52–58], masses settled on the network's vertices interact with each other through a spring with a uniform spring constant. This mass–spring model and the associated powerful analytical method, normal mode analysis, which were originally developed in classical mechanics [52, 53], have been extensively used in many other disciplines, such as protein dynamics in structural biology [54] and lattice vibrations and associated phonon excitations in solid-state physics [55]. In this paper, we will study the same optimal configuration problem but turn to the regular ring structure [51]. As now the node degree is homogeneous, some previous interesting findings on sufficiently random networks depending on the matching between the node degree and node parameter disappear, but some other unusual phenomena purely depending on the spatial position of masses are expected.

The paper is organized as follows. In Section 2, the model and some theoretical results for very small system sizes are presented. In Section 3, all numerical results including $(\omega_2)_{\min}$, $(\omega_2)_{\max}$, $(\omega_N)_{\min}$, and $(\omega_N)_{\max}$ for very large system sizes relying on our observations are given in detail. Finally, the last section is devoted to a brief discussion and our conclusion.

2 Model and analysis

For the simplest case of spatial structure, i.e., the nearest-neighbor-coupled ring configuration, the equations of motion are

$$m_j\ddot{x}_j = \kappa(x_{j+1} + x_{j-1} - 2x_j), \quad j = 1, \ldots, N, \tag{1}$$

where m_j represents the jth oscillator's mass, κ is the spring constant, and N indicates the number of mass points. Without loss of generality, we take $\kappa \equiv 1$ throughout this paper. Periodic boundary conditions, i.e., $x_{N+1} = x_1$ and $x_0 = x_N$, are always used. Because we are interested in the spatial distribution effect of different masses, we always consider distinct masses m_j for all j's; i.e., all masses are nonidentical.

Based on normal mode analysis, the system's motion can be considered as a linear superposition of N normal modes with different characteristic frequencies:

$$x_j = \sum_{i=1}^{N} y_j e^{\mathrm{i}\omega_i t}, \tag{2}$$

where ω_i and y_j denote an independent characteristic frequency and its corresponding amplitude, respectively. The frequencies can be ordered as $\omega_1 \leqslant \omega_2 \leqslant \cdots \leqslant \omega_N$. Clearly, $\omega_1 = 0$ represents the translational motion of the system. Among all the modes, the second smallest

(slowest) vibration frequency ω_2 characterizes the most global vibrational motion, whereas the largest vibration frequency ω_N reflects the most tightly packed and constrained local motion generally; both of them are the most representative. Therefore, as in our previous work on the vibration frequencies on complex networks [51], we will only consider these two characteristic frequencies ω_2 and ω_N and study how they are determined by the different mass spatial configurations.

For small sizes, $N = 2$ and $N = 3$, the vibration spectra are explicitly available and are, respectively,

$$\omega = \begin{bmatrix} 0 \\ \sqrt{\dfrac{m_1 + m_2}{m_1 m_2}} \end{bmatrix} \tag{3}$$

and

$$\omega = \begin{bmatrix} 0 \\ \sqrt{\dfrac{m_1m_2 + m_1m_3 + m_2m_3 - \sqrt{m_1^2m_2^2 + m_1^2m_3^2 + m_2^2m_3^2 - m_1m_2m_3(m_1 + m_2 + m_3)}}{m_1m_2m_3}} \\ \sqrt{\dfrac{m_1m_2 + m_1m_3 + m_2m_3 + \sqrt{m_1^2m_2^2 + m_1^2m_3^2 + m_2^2m_3^2 - m_1m_2m_3(m_1 + m_2 + m_3)}}{m_1m_2m_3}} \end{bmatrix}. \tag{4}$$

Clearly, for the simplest case ($N = 2$) with only two masses m_1 and m_2 connected by a spring, the physical quantity $\mu = \frac{m_1m_2}{m_1+m_2}$ is the effective mass of the system; it solely determines the only nonzero vibration frequency: $\omega_2 = \omega_N = 1/\sqrt{\mu}$.

For $N = 3$ in Eq. (4), clearly the second smallest and the largest vibration frequencies ω_2 and ω_3 are complicated functions of the mass values. However, because of the periodic boundary conditions, only one independent configuration exists. Thus, the transform of any two masses among m_1, m_2, and m_3 will not change the values of ω_2 and ω_3; this point is clear in Eq. (4).

For $N = 4$, with the aid of symbol calculation using the MATLAB software, we can also obtain an explicit expression for all vibration frequencies, but the equation is too lengthy to be presented here. For $N > 4$, even MATLAB cannot give an explicit expression using a personal computer. We surmise that, even if more powerful computers could give an explicit expression for much larger N, finding useful rules from the complicated and lengthy algebraic function would be difficult. Therefore, to accomplish our goal, we have to turn to numerical simulations and try to find some general results from the numerical results.

The above equations [Eqs. (1)] can be written in the compact form

$$(\omega^2 M - L)Y = 0, \tag{5}$$

where $M = \mathrm{diag}(\{m_j\})$, L is the Laplacian matrix: $L(i,i) = 2$, $L(j,i) = -1$ for $|j - i| = 1$ or $N - 1$ and $L(j,i) = 0$ otherwise, and Y is the N-dimensional nonzero column vector with the components y_i in (2).

Solving Eq. (5) is equivalent to finding ω satisfying $\det(\omega^2 M - L) = 0$, where "det" denotes the determinant. For M being nonsingular, it is convenient to change the mass-weighted Laplacian matrix to a symmetric one; this manipulation does not change the final result, but it becomes more efficient in simulations to solve eigenvalues of a symmetric matrix than those of an asymmetric matrix. Therefore, we have

$$\omega^2 = \lambda(M^{-1}L) = \lambda(M^{-1/2}LM^{-1/2}), \tag{6}$$

where λ denotes the eigenvalue of the corresponding matrix.

For choosing the masses, we assume that the units are ordered with increasing weight $m_1 \leqslant m_2 \leqslant \cdots \leqslant m_N$ and that they are denoted as $1, 2, \ldots, N$, correspondingly. It is easy to see that the number of independent mass spatial configurations for a ring consisting of N distinct masses is $(N-1)!/2$, which diverges with N and is certainly beyond the feasible limit of our computational resources for any large N. Therefore, our strategy is to begin by inferring the optimal configuration rules by exhaustively searching all the spatial configurations for sufficiently small N first (e.g., $N \leqslant 10$) and then apply and verify these rules for much larger N. When the precise rules for the optimal configurations for ω_2 and ω_N are not available by our analysis, some approximate rules are also highly appreciated. However, we start from the simplest nonidentical case, namely, the case in which all the masses are completely linearly distributed, $m_i = i$ for $i = 1, \ldots, N$. Later, we will generalize this case to more complicated random distributions of masses.

For a set of fixed masses and a given configuration, the vibration frequencies can be easily calculated from the above eigenvalue analysis in Eq. (6). Below we will focus on the two most representative frequencies ω_2 and ω_N, scrutinize their corresponding optimal configurations for $(\omega_2)_{\min}$, $(\omega_2)_{\max}$, $(\omega_N)_{\min}$, and $(\omega_N)_{\max}$, and present the numerical results and our observations in more detail in

the next section.

3 Numerical results and observations

3.1 $(\omega_2)_{\min}$

Figures 1(a)–(h) present the numerical results of ω_2 in ascending order for all the mass spatial configurations for $N = 3, \ldots, 10$, respectively. In addition, we depict the mass spatial configurations for the first several smallest ω_2's under each subfigure. For these configurations, ω_2 increases from left to right and the configuration for $(\omega_2)_{\min}$ is the first one. The numbers around the ring represent the orders of the masses (or, equivalently, the values of the masses).

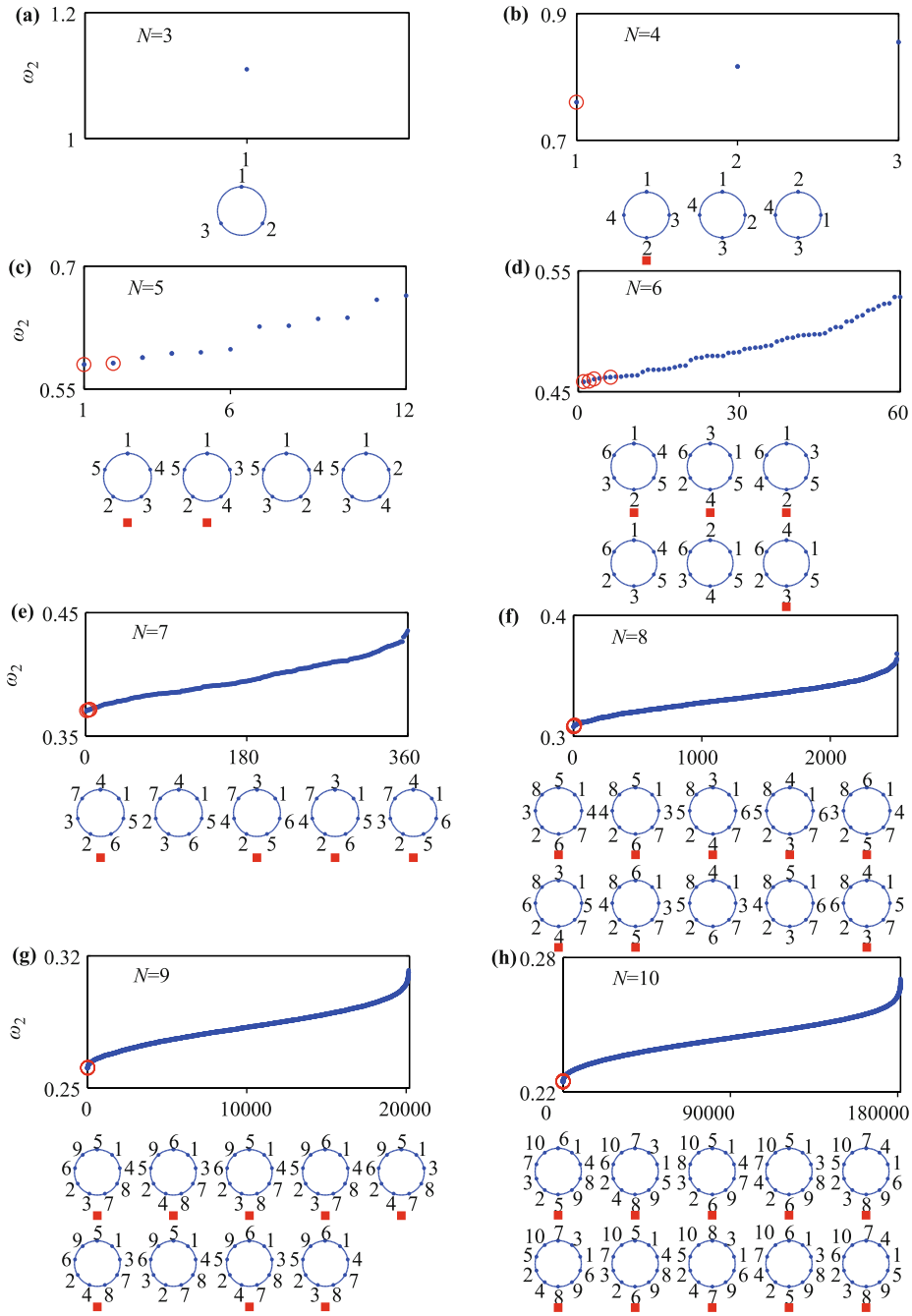

Fig. 1 **(a)–(h)** Plots of ω_2 arranged in ascending order for all mass spatial configurations of nonidentical masses located on a ring for $N = 3, \cdots, 10$, respectively. All masses are denoted by $1, \cdots, N$ in ascending order in respect to their masses. Under each sub-plot, we present the first several configurations for small values of ω_2, and mark the configuration by a red filled square if it satisfies the grouping rules. Its corresponding value is emphasized by a red open circle in the sub-plot, which definitely shows that their values are indeed very small.

Our objective is to find the common organizing rule for $(\omega_2)_{\min}$. By carefully observing these mass spatial configurations in Fig. 1, we do find some common rules, which are described as follows. (To aid explanation, two examples for $N = 8$ and $N = 9$ are shown in Fig. 2.) When N is even, any two closest masses can be put into a group successively to form a mass pair, i.e., $\{\{m_1, m_2\}, \{m_3, m_4\}, \ldots, \{m_{2i-1}, m_{2i}\}, \ldots, \{m_{N-1}, m_N\}\}$. Then, any pair should be placed on the two sides of the diameter of the ring and the masses in any one pair can exchange their positions. Thus, any two masses in each pair show diametral symmetry. Finally, the pair position could be determined. We may denote an arbitrary mass spatial configuration as $a(j)$ and the mass of the jth configuration rearranged as $m_i^{a(j)} = m_{i(j)}$. The pair spatial configuration corresponding to the minimal ω_2 should maximize the following physical quantity:

$$R = \sum_{i=1}^{[(N+1)/2]} m_i^a m_{i+1}^a, \tag{7}$$

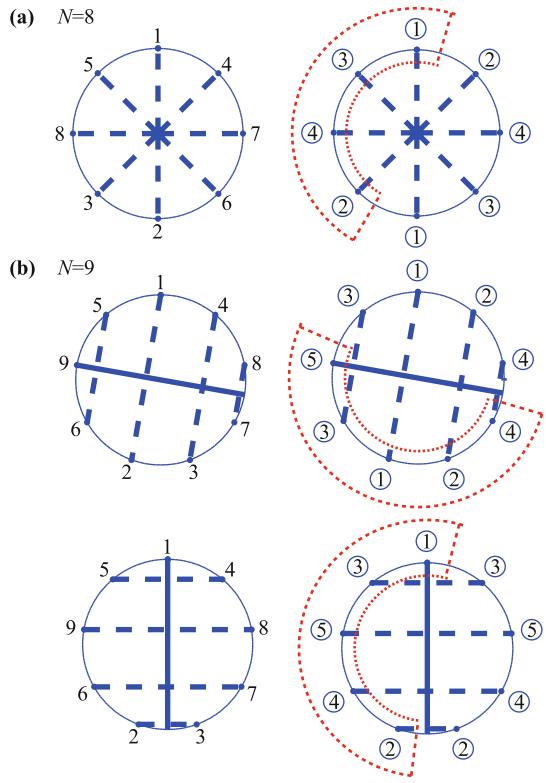

Fig. 2 **(a)** and **(b)** Schematic shows for the grouping rules of $(\omega_2)_{\min}$ for even and odd N's, respectively. The circled numbers in the right column denote the "effective" mass in a mass pair after grouping, whose position can be further determined by Eq. (7). Clearly for even N, the pattern shows the diametral symmetry, whereas it shows mirror symmetry for odd N. In addition, we can uniquely determine the specific configuration of $(\omega_2)_{\min}$ for odd N, after applying the grouping rule from the lightest mass side one more time, as shown in the bottom patterns of (b). For more details, see the text.

where $[j]$ represents the nearest integer less than or equal to j.

Based on such observations, for even N we can only have the above grouping rules and actually we cannot precisely determine the configuration for $(\omega_2)_{\min}$, which is only one among all possible grouping configurations. Hereafter, we use $(\omega_2)_{\min,G}$ to denote the configurations satisfying the grouping rules. See the schematic shown for $N = 8$ in Fig. 2(a) for further details, and check the configurations in Fig. 1, where red filled squares are used to indicate the configurations for groupings and red open circles for their corresponding values of ω_2. From these plots, remarkably all values of $(\omega_2)_{\min,G}$ have been greatly squeezed into a very small regime. Thus, we have captured the essential rules for $(\omega_2)_{\min}$ by $(\omega_2)_{\min,G}$, although we cannot recognize the exact one corresponding to $(\omega_2)_{\min}$. As we will see below, these rules also work for odd N with some variations.

When N is odd, the mass pairs become $\{\{m_1, m_2\}, \ldots, \{m_{N-2}, m_{N-1}\}, \{m_N\}\}$, and we have to fix the unmatched heaviest mass first. Then, any mass pairs should be placed (mirror) symmetrically about the diameter for the heaviest mass. See the schematic shown for $N = 9$ in Fig. 2(b) for further details. We use the solid line to emphasize the main diameter starting from the heaviest mass m_9 and the dashed lines for the paired masses showing mirror symmetry. As for even N, any two masses in any pair can exchange their positions, and their corresponding ω_2 values are of very small difference and are essentially indistinguishable. Interestingly, the mass pair arrangement condition for maximizing R in Eq. (7) also works here. Considering these grouping procedures, we can obtain the independent number of configurations $2^{[N/2]-1}$ for $N > 4$, irrespective of N being even or odd, and 1 for $N = 4$.

For N being odd, some other variations exist. Actually, for odd N, we can further precisely determine the configuration for $(\omega_2)_{\min}$ as we can group the whole masses from the other side, namely, $\{\{m_1\}, \{m_2, m_3\}, \ldots, \{m_{N-1}, m_N\}\}$. In this situation, the lightest mass becomes the isolated one. Similarly, we can fix the unmatched lightest unit m_1 and place all other mass pairs mirror-symmetrically with the diameter starting from it. Consequently, the specific configuration for $(\omega_2)_{\min}$ can be fully determined; the two different grouping schemes for $(\omega_2)_{\min}$ are exemplified in Fig. 2(b) for $N = 9$.

Until now, the rules for $(\omega_2)_{\min,G}$ for any N and $(\omega_2)_{\min}$ for odd N have been found on the basis of observations on small N. Below we check these rules for large N. For this purpose, Fig. 3(a) depicts the numerical results of ω_2 in ascending order for completely random

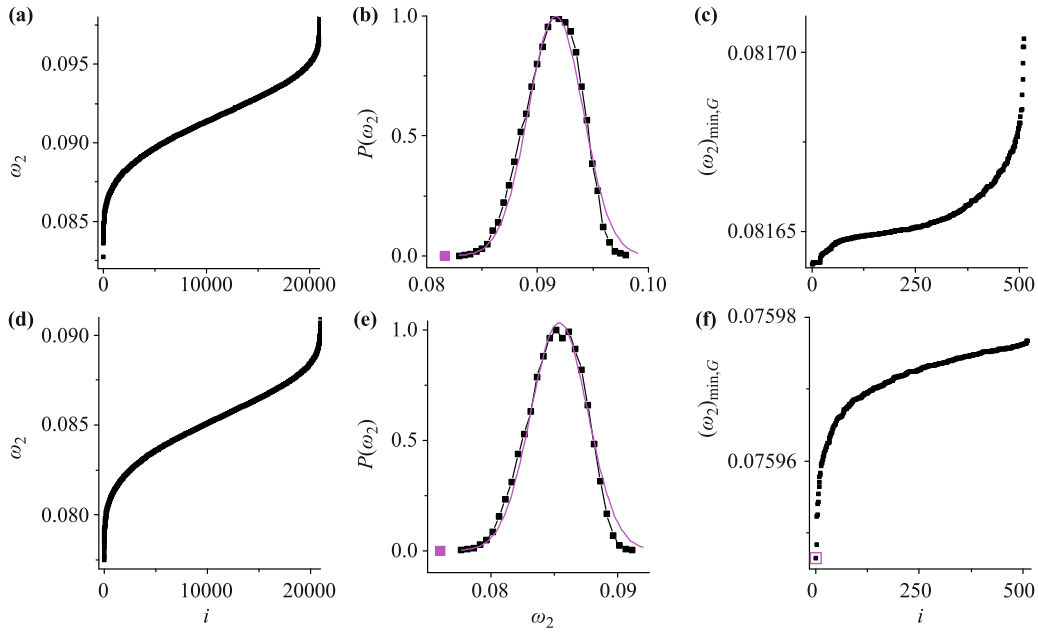

Fig. 3 **(a)** and **(b)** Plots of ω_2 in ascending order for completely random 20000 configurations and their histogram distribution; $N = 20$. (c) Plot of $(\omega_2)_{\min,G}$ in ascending order for exhausting searching all 512 configurations satisfying the grouping rules, clearly showing that their values are very small. In (b), the fit is a Gaussian function (red line), and the group mean value, $\langle(\omega_2)_{\min,G}\rangle$, is located at the leftmost of the distribution (red filled square). **(d)**–**(f)** Similar to (a)–(c) but for $N = 21$ instead; under this situation for odd N, we can determine the specific configuration of $(\omega_2)_{\min}$, whose value $(\omega_2)_{\min}$ is indicated by the red open square in (f).

spatial configurations for $N = 20$. A sufficiently large number of configurations, 20000, is selected. The corresponding histogram distribution, presented in Fig. 3(b), is indicative of a Gaussian distribution (red curve). Clearly, ω_2 has a wide distribution, ranging from $\omega_2 \approx 0.083$ to $\omega_2 \approx 0.098$. In addition, we select all $(2^{[20/2]-1} = 512)$ configurations for ω_2 satisfying the grouping rules and plot their corresponding values of ω_2 in Fig. 3(c). Remarkably, the values of ω_2 in the group have been greatly squeezed into a much smaller regime: $0.08164 < \omega_2 < 0.08171$. Note the different scales employed in Figs. 3(a) and (c) and the range of ω_2's in Fig. 3(c) being only 1/200 that of the original range in Fig. 3(a). Additionally, the mean value, $\langle(\omega_2)_{\min,G}\rangle$, marked with a red filled square in Fig. 3(b), is clearly located at the leftmost of the distribution. Here $\langle\ldots\rangle$ denotes the mean value over sufficiently large tests. All these figures obviously prove the grouping organization rules of ω_2, although the common rule of the exact configuration for $(\omega_2)_{\min}$ for even N is missing.

Similarly, Figs. 3(d)–(f) show the results for $N = 21$. As now the configuration for $(\omega_2)_{\min}$ can be precisely determined, its value is signaled by a red open square in Fig. 3(f), being the lowest in the whole distribution of $(\omega_2)_{\min,G}$. Again, this perfectly proves our prediction.

For N being sufficient large, e.g., $N = 50$ and $N = 51$, $\langle(\omega_2)_{\min,G}\rangle$ and $(\omega_2)_{\min}$ have the same patterns as ω_2 in Fig. 3. (The figures are not presented here.) All these results confirm our predictions for sufficiently large N. Finally, we have also calculated the average values for ω_2 and $(\omega_2)_{\min,G}$ for different N's and $(\omega_2)_{\min}$ for odd N's only. These results show that they all damp, exhibiting a power-law relation with similar scales as a function of N. The results also indicate that the mismatch between $(\omega_2)_{\min,G}$ [or $(\omega_2)_{\min}$] and ω_2 becomes diminishing with increasing N.

3.2 $(\omega_2)_{\max}$

So far, we have successfully obtained the rules for $(\omega_2)_{\min}$. Next, let us see what happens for $(\omega_2)_{\max}$. Similar to Fig. 1, Fig. 4 is for ω_2's but focuses on the configurations for large ω_2 instead. In all these configurations, ω_2 increases from left to right and the last one corresponds to $(\omega_2)_{\max}$. After carefully observing these spatial configurations, we can conclude only that all these configurations have rough bipartite characteristics; namely, the heaviest masses like to gather together on one side of the ring, while the lightest ones gather on the other side. We fail to obtain the controlling rules for $(\omega_2)_{\max}$ or even $(\omega_2)_{\max,G}$.

3.3 $(\omega_N)_{\min}$

Now, let us turn to the study of $(\omega_N)_{\min}$. Similar to what we have done for ω_2, we calculated ω_N's exhaustedly

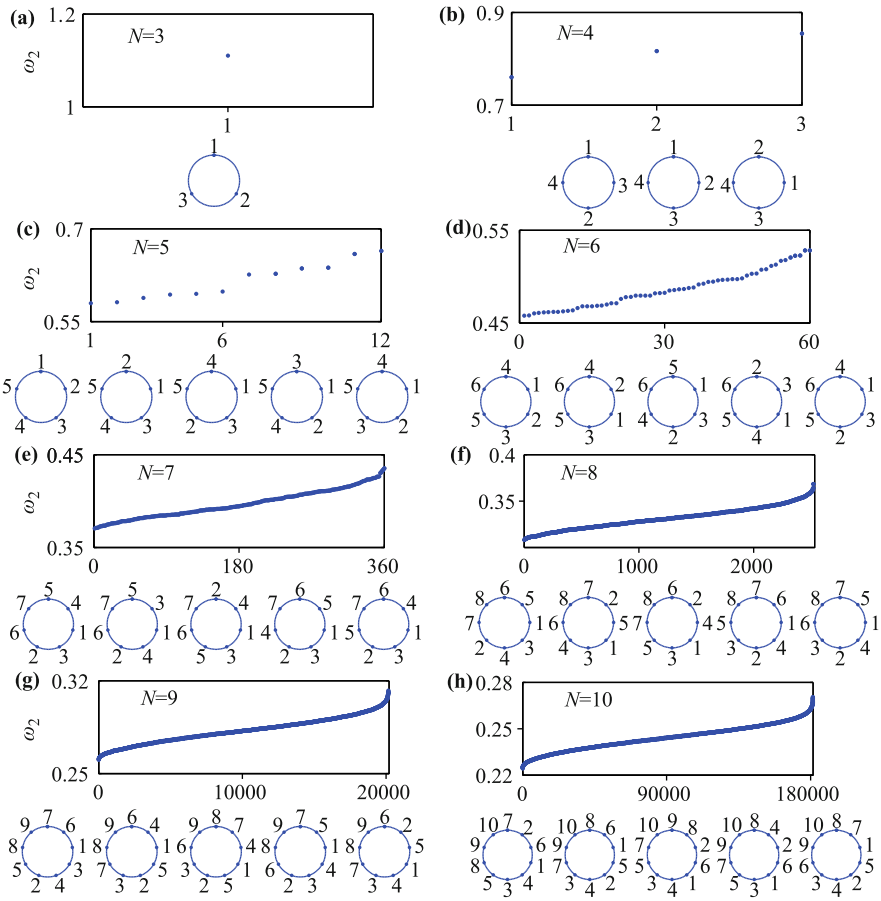

Fig. 4 Similar to Fig. 1, but focusing on the configurations from the large side of ω_2 instead. The rightmost pattern corresponds to $(\omega_2)_{\max}$. Here roughly the heavy masses are located on one side of the ring, and the light masses on the other side, and no any specific rules are available.

for all different configurations for $N = 3, \ldots, 10$; the results are presented in Figs. 5(a)–(h). Again, the specific mass spatial configurations for several small ω_N's are illustrated in ascending order. A key distinction from the case for ω_2 in Fig. 1 is that the distribution now becomes noncontinuous, accompanied with some breaks.

Similarly, we have to derive the underlying rules from these patterns. Without loss of generality, again we take $N = 8$ and $N = 9$ as two examples in Fig. 6. For $N = 8$ in Fig. 6(a), we may divide the units into pairs, $\{\{m_1, m_2\}, \{m_3, m_4\}, \ldots, \{m_{2i-1}, m_{2i}\}, \ldots, \{m_{N-1}, m_N\}\}$, whereas for $N = 9$, $\{\{m_1\}, \{m_2, m_3\}, \ldots, \{m_{2i}, m_{2i+1}\}, \ldots, \{m_{N-1}, m_N\}\}$. Clearly, for $N = 8$, the lightest mass pair (masses m_1 and m_2) are fixed on one diameter of a ring (solid line), whereas any two masses in the pair are placed mirror-symmetrically about the solid line. To emphasize the mirror symmetry relation, we have connected them by several dashed lines. However, for $N = 9$, the unmatched lightest one starting from m_1 is emphasized by the solid line, and any two masses in one pair are also placed symmetrically about the solid line. In addition, we find that the mass pairs are listed in ascending order; see, e.g., $\{1, 2, 3, 4\}$ in the right column of Fig. 6(a) for $N = 8$ and $\{1, 2, 3, 4, 5\}$ in the right column of Fig. 6(b) for $N = 9$. Namely, the pair positions are fixed in the ring. We also find that, irrespective of whether N is even or odd, the lightest node with mass m_1 is always placed between the two heaviest nodes with masses m_{N-1} and m_N; this feature persists for more general sets of masses, as we will see below. Here it is noticeable that we cannot determine the configuration for $(\omega_N)_{\min}$ even if N is odd.

Therefore, based on the above observations, the optimal configurations for the approximate $(\omega_N)_{\min}$ in the grouping manner can be easily obtained, although the precise configuration for $(\omega_N)_{\min}$ is not available for any N. We may denote all these possible configurations for small ω_N as $(\omega_N)_{\min,G}$. It is also quite interesting to recognize that the number of independent configurations is the same as in the case for $(\omega_2)_{\min,G}$, namely, $2^{[N/2]-1}$ for $N > 4$, irrespective of N being even or odd, and 1 for $N = 4$.

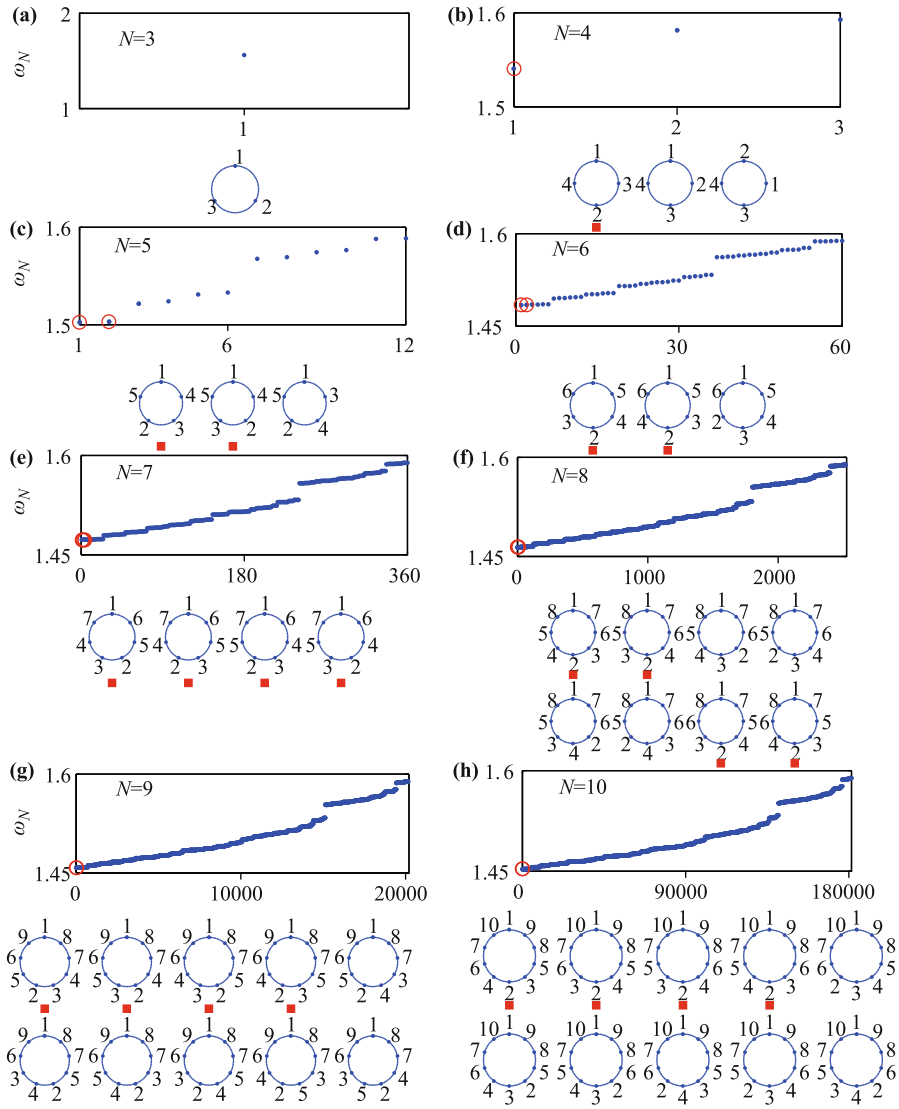

Fig. 5 Similar to Fig. 1 but for $(\omega_N)_{\min}$ instead. Similarly, the configurations satisfying the grouping rule are denoted by the solid squares in the configuration plots and the corresponding value of ω_N by the open circles in the distribution plots. Note that here the grouping rule is different.

3.4 $(\omega_N)_{\max}$

Now we focus on the case of large ω_N and their corresponding mass spatial configurations in Fig. 7. By thoroughly investigating the last configurations for $(\omega_N)_{\max}$ in Figs. 7(a)–(h) for each N, we can find that they just correspond to the maximal value of the physical quantity

$$R = \sum_{i=1}^{N} m_i^a m_{i+1}^a, \tag{8}$$

where $m_{N+1}^a = m_1^a$ for the periodic boundary condition. Note the key difference from the similar equation [Eq. (7) for $(\omega_2)_{\min}$]: Now the summarization is from 1 to N for all nodes. Luckily, we can obtain the optimal configuration for $(\omega_N)_{\max}$ for any N, without needing to consider grouping rules for approximate extreme values again. Figures 8(a) and (b) give schematic views of $(\omega_N)_{\max}$ for $N = 8$ and $N = 9$, respectively. Although now the grouping rules are unnecessary, we may still divide all the nodes into several groups with similar masses and show the mirror symmetry for both $N = 8$ and $N = 9$, as illustrated in the two bottom configurations of the figures.

Finally, all these organization rules for $(\omega_N)_{\min}$ and $(\omega_N)_{\max}$ have been well checked for large N, as shown in Figs. 9(a)–(d) for $N = 20$, 21, 50, and 51, where the ragged, noncontinuous patterns are clear and the values of $\langle(\omega_N)_{\min,G}\rangle$ (red filled squares) and $(\omega_N)_{\max}$ (red open squares) always remain at the leftmost and rightmost sides of the distributions for all N's. In addition,

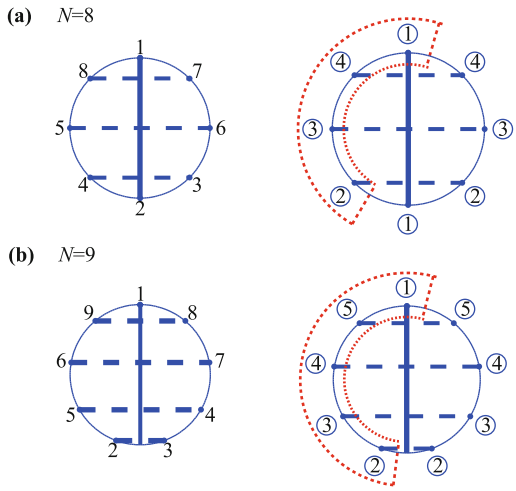

Fig. 6 **(a)** and **(b)** Schematic shows for the grouping rules of $(\omega_N)_{\min}$ for even and odd N's, respectively. Under this situation, the mirror symmetry works for all N's. In addition, for odd N only the grouping configurations (starting from the lightest mass m_1), $(\omega_N)_{\min,G}$, are available, but not $(\omega_N)_{\min}$. For more details, see the text.

we have also calculated the values of $\langle\omega_N\rangle$, $\langle(\omega_N)_{\min,G}\rangle$, and $(\omega_N)_{\max}$ as a function of N. The results clearly show the damping relation for $\langle\omega_N\rangle$ and $\langle(\omega_N)_{\min,G}\rangle$, along with a nearly unchanging relation for $(\omega_N)_{\max}$, indicative of a quite different pattern with ω_2.

3.5 General cases

So far, we have obtained the mass spatial configuration rules for an exact linear distribution of $\{m_i\}$. Below we consider more general situations for the node masses. For example, the values of m_i for $i = 1, \ldots, N$ are uniformly, randomly chosen from the interval $(0, 1)$. We found that some rules still hold, but some others disappear: (i) For $(\omega_2)_{\min}$, the same grouping rules remain. However, we can only obtain the general group $(\omega_2)_{\min,G}$ but not the specific minimum for N being odd, as shown by the configurations in Fig. 2(a) and the top configurations in Fig. 2(b). (ii) For $(\omega_2)_{\max}$, still only the approximate bipartite

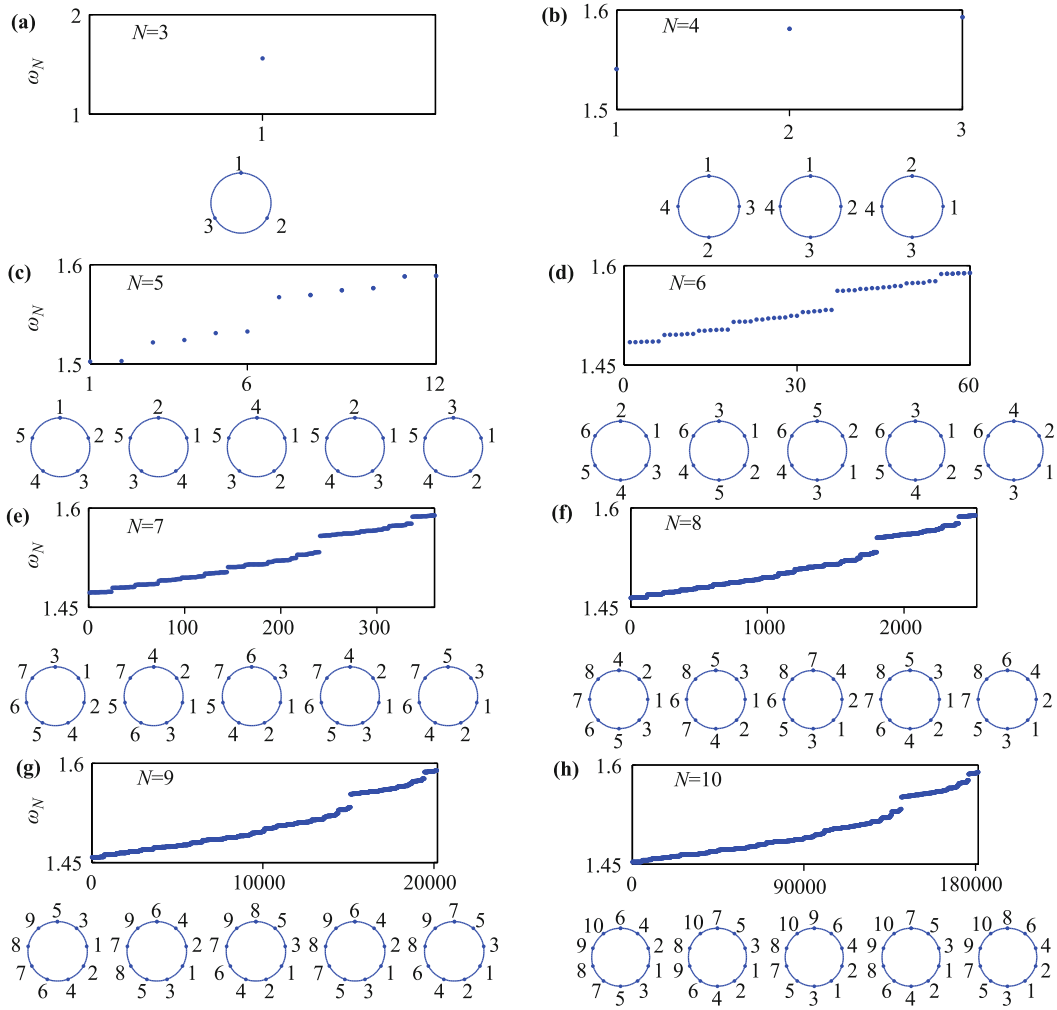

Fig. 7 Similar to Fig. 5 but on the large side of ω_N. The configuration for $(\omega_N)_{\max}$ can be specifically obtained.

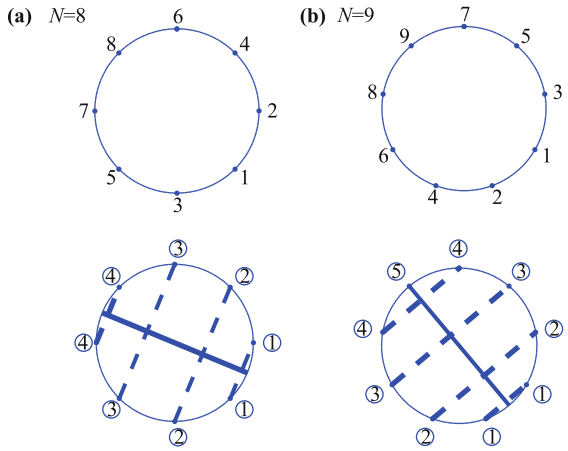

Fig. 8 **(a)** and **(b)** Spatial configurations of $(\omega_N)_{\max}$ for $N = 8$ and $N = 9$, respectively. Now its configuration can be specifically obtained for any N. In addition, we may view them with the mirror-symmetry grouping rules, as shown in the bottom configurations.

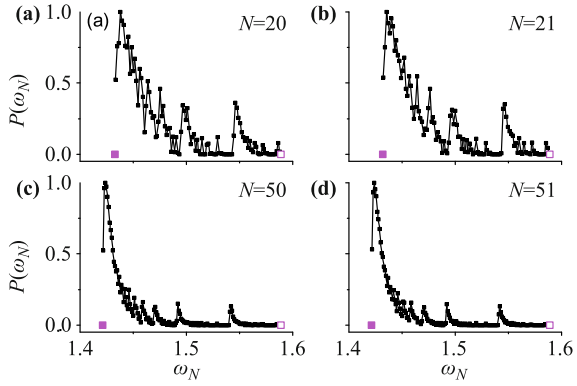

Fig. 9 **(a)**–**(d)** Histograms of ω_N for different N's: $N = 20$, 21, 50, and 51, respectively, showing the similar non-continuous, asymmetric distributions. The red solid and open squares denote $\langle(\omega_N)_{\min,G}\rangle$ and $(\omega_N)_{\max}$, respectively, from our predictions.

distribution is available. (iii) For $(\omega_N)_{min}$, the feature for the lightest node placed between the two heaviest nodes persists, as shown by the fractions of the positions $\{8, 1, 7\}$ and $\{9, 1, 8\}$ in Figs. 6(a) and (b), respectively, while all other grouping rules disappear. (iv) For $(\omega_N)_{\max}$, luckily all the rules persist. Furthermore, we have found that all these rules are unchanged for many other tests for randomly chosen m_i's and hold not only for the ring configuration with the nearest-neighboring connections but also for longer local connections with ranges of 2 or 3. Therefore, these properties are expected to be very general for any regular network.

4 Discussion and conclusions

In conclusion, we have investigated the parameter diversity effect of coupled harmonic oscillators with different masses on a regular ring network and discovered the organization rules for the spatial configurations of the masses for the extreme values of ω_2 and ω_N. It has been shown that symmetric rules and grouping rules are both very important in determining the whole system dynamics on the regular ring. This is a key distinction from our previous studies on coupled networked harmonic oscillators [51], for which the matching between the node parameter and the node degree on complex networks is extremely important.

We summarize the symmetric rules and grouping rules for the optimal configurations for the special case with $m_i = i$ in Table 1, where G indicates that we can find grouping spatial configurations, O indicates that we can find a specific optimal configuration, and R indicates that we have only rough (nonspecific) rules. In addition, the letters DS, MS, and NS indicate that the grouped masses have diametral symmetry, mirror symmetry, and no symmetry, respectively. Additionally, we also present the organization rules for the general cases for randomly chosen m_i values in Table 2.

Table 1 Vibration frequencies for a special case, where $m_i = i$ for $i = 1, \ldots, N$. Here G represents that we can find grouping spatial configurations, O indicates that we can find the specific optimal configuration, and R denotes that we have only rough (not specific) rules. In addition, the letters DS, MS, and NS indicate that the grouped masses have the features: diametral symmetry, mirror symmetry, and no symmetry, respectively. See the text for more details.

	N is Even	N is Odd
$(\omega_2)_{\min}$	G (DS) [Fig. 2(a)]	O (MS) [Fig. 2(b)]
$(\omega_2)_{\max}$	R (NS) [Fig. 4]	R (NS) [Fig. 4]
$(\omega_N)_{\min}$	G (MS) [Fig. 6(a)]	G (MS) [Fig. 6(b)]
$(\omega_N)_{\max}$	O (MS) [Fig. 8(a)]	O (MS)[Fig. 8(b)]

Table 2 Vibration frequencies for general cases, where m_i's are randomly chosen. See text for more details.

	N is Even	N is Odd
$(\omega_2)_{\min}$	G (DS)	G (MS)
$(\omega_2)_{\max}$	R (NS)	R (NS)
$(\omega_N)_{\min}$	R (NS)	R (NS)
$(\omega_N)_{\max}$	O (MS)	O (MS)

These findings might be applicable for explaining some interesting phenomena in realistic systems, such as lattice vibrations and associated excitations in atomic or molecular systems. In addition, the optimal configuration exhibits the significance of symmetry (including mirror symmetry, diametric symmetry, and no symmetry) and grouping between nodes with similar parameters (masses), which may help us to further understand the parameter diversity effect and may provide us with potential guidelines in engineering design. We expect

these findings could arouse general interest in studying the diversity-induced effect and the structure-dynamics-function relation in complex systems, both of which are of fundamental importance for deciphering and utilizing the spontaneous order in nature and in human-made products.

Acknowledgements This work was supported by the National Natural Science Foundation of China under Grant Nos. 11075202 and 11475253.

References

1. Y. Bar-Yam, Dynamics of Complex Systems, Westview Press, 1997
2. M. E. J. Newman, Networks: An Introduction, Oxford University Press, 2009
3. I. Rigoutsos and G. Stephanopoulos, Systems Biology (Volume II): Networks, Models, and Applications, Oxford University Press, USA, 2006
4. I. N. Serdyuk, Methods in Molecular Biophysics: Structure, Dynamics, Function, Cambridge University Press, 2007
5. T. P. Trappenberg, Fundamentals of Computational Neuroscience, Oxford University Press, 2010
6. S. Boccaletti, The Synchronized Dynamics of Complex Systems, Elsevier Science, 2008
7. S. Boccaletti, V. Latora, Y. Moreno, M. Chavez, and D. U. Hwang, Complex networks: Structure and dynamics, *Phys. Rep.* 424(4–5), 175 (2006)
8. R. Albert and A. L. Barabàsi, Statistical mechanics of complex networks, *Rev. Mod. Phys.* 74(1), 47 (2002)
9. A. Arenas, A. Díaz-Guilera, J. Kurths, Y. Moreno, and C. Zhou, Synchronization in complex networks, *Phys. Rep.* 469(3), 93 (2008)
10. S. N. Dorogovtsev, A. V. Goltsev, and J. F. Mendes, Critical phenomena in complex networks, *Rev. Mod. Phys.* 80(4), 1275 (2008)
11. S. Liu, Z. W. He, and M. Zhan, Firing rates of coupled noisy excitable elements, *Front. Phys.* 9(1), 120 (2014)
12. P. Ke and Z. Zheng, Dynamics of rotator chain with dissipative boundary, *Front. Phys.* 9(4), 511 (2014)
13. X. Y. Wu and Z. G. Zheng, Hierarchical cluster-tendency analysis of the group structure in the foreign exchange market, *Front. Phys.* 8(4), 451 (2013)
14. Z. Q. Yuan and Z. G. Zheng, Propagation dynamics on the Fermi-Pasta-Ulam lattices, *Front. Phys.* 8(3), 349 (2013)
15. L. M. Pecora and T. L. Carroll, Master stability functions for synchronized coupled systems, *Phys. Rev. Lett.* 80(10), 2109 (1998)
16. J. Yang, G. Hu, and J. Xiao, Chaos synchronization in coupled chaotic oscillators with multiple positive Lyapunov exponents, *Phys. Rev. Lett.* 80(3), 496 (1998)
17. G. Wei, M. Zhan, and C. H. Lai, Tailoring wavelets for chaos control, *Phys. Rev. Lett.* 89(28), 284103 (2002)
18. M. Zhan, G. Hu, and J. Yang, Synchronization of chaos in coupled systems, *Phys. Rev. E* 62(2), 2963 (2000)
19. A. E. Motter, C. Zhou, and J. Kurths, Network synchronization, diffusion, and the paradox of heterogeneity, *Phys. Rev. E* 71(1), 016116 (2005)
20. C. Zhou, A. E. Motter, and J. Kurths, Universality in the synchronization of weighted random networks, *Phys. Rev. Lett.* 96(3), 034101 (2006)
21. M. Chavez, D. U. Hwang, A. Amann, H. Hentschel, and S. Boccaletti, Synchronization is enhanced in weighted complex networks, *Phys. Rev. Lett.* 94(21), 218701 (2005)
22. X. Wang, Y. C. Lai, and C. H. Lai, Enhancing synchronization based on complex gradient networks, *Phys. Rev. E* 75(5), 056205 (2007)
23. S. Liu and M. Zhan, Clustering versus non-clustering phase synchronizations, *Chaos: An Interdisciplinary J. Nonlinear Sci.* 24, 013104 (2014)
24. K. Wiesenfeld, C. Bracikowski, G. James, and R. Roy, Observation of antiphase states in a multimode laser, *Phys. Rev. Lett.* 65(14), 1749 (1990)
25. M. Zhan, G. Hu, Y. Zhang, and D. He, Generalized splay state in coupled chaotic oscillators induced by weak mutual resonant interactions, *Phys. Rev. Lett.* 86(8), 1510 (2001)
26. W. Zou and M. Zhan, Splay states in a ring of coupled oscillators: From local to global coupling, *SIAM J. Appl. Dyn. Syst.* 8(3), 1324 (2009)
27. D. Aronson, G. Ermentrout, and N. Kopell, Amplitude response of coupled oscillators, *Physica D* 41(3), 403 (1990)
28. W. Zou and M. Zhan, Partial time-delay coupling enlarges death island of coupled oscillators, *Phys. Rev. E* 80(6), 065204 (2009)
29. W. Zou, X. Zheng, and M. Zhan, Insensitive dependence of delay-induced oscillation death on complex networks, *Chaos: An Interdisciplinary J. Nonlinear Sci.* 21, 023130 (2011)
30. P. Bak, How Nature Works: The Science of Self-Organized Criticality, Vol. 212, New York: Copernicus, 1996
31. W. Ren, R. W. Beard, and E. M. Atkins, A survey of consensus problems in multi-agent coordination, American Control Conference, 2005, Proceedings of the 2005 (IEEE), 1859–1864 (2005)
32. R. Pastor-Satorras and A. Vespignani, Epidemic spreading in scale-free networks, *Phys. Rev. Lett.* 86(14), 3200 (2001)
33. G. Filatrella, A. H. Nielsen, and N. F. Pedersen, Analysis of a power grid using a Kuramoto-like model, *Eur. Phys. J. B* 61(4), 485 (2008)
34. A. E. Motter, S. A. Myers, M. Anghel, and T. Nishikawa, Spontaneous synchrony in power-grid networks, *Nat. Phys.* 9(3), 191 (2013)
35. P. J. Menck, J. Heitzig, J. Kurths, and H. J. Schellnhuber, How dead ends undermine power grid stability, *Nat. Commun.* 5, 3969 (2014)

36. Y. Braiman, J. F. Lindner, and W. L. Ditto, Taming spatiotemporal chaos with disorder, *Nature* 378(6556), 465 (1995)

37. S. de Monte, F. d'Ovidio, and E. Mosekilde, Coherent regimes of globally coupled dynamical systems, *Phys. Rev. Lett.* 90(5), 054102 (2003)

38. S. F. Brandt, B. K. Dellen, and R. Wessel, Synchronization from disordered driving forces in arrays of coupled oscillators, *Phys. Rev. Lett.* 96(3), 034104 (2006)

39. C. Zhou, J. Kurths, and B. Hu, Array-enhanced coherence resonance: Nontrivial effects of heterogeneity and spatial independence of noise, *Phys. Rev. Lett.* 87(9), 098101 (2001)

40. C. J. Tessone, C. R. Mirasso, R. Toral, and J. D. Gunton, Diversity-induced resonance, *Phys. Rev. Lett.* 97(19), 194101 (2006)

41. R. Toral, C. J. Tessone, and J. V. Lopes, Collective effects induced by diversity in extended systems, *Eur. Phys. J. Spec. Top.* 143(1), 59 (2007)

42. C. J. Tessone and R. Toral, Diversity-induced resonance in a model for opinion formation, *Eur. Phys. J. B* 71(4), 549 (2009)

43. A. Szolnoki, M. Perc, and G. Szabó, Diversity of reproduction rate supports cooperation in the prisoner's dilemma game on complex networks, *Eur. Phys. J. B* 61(4), 505 (2008)

44. M. Brede, Synchrony-optimized networks of non-identical Kuramoto oscillators, *Phys. Lett. A* 372(15), 2618 (2008)

45. S. Acharyya and R. E. Amritkar, Synchronization of coupled nonidentical dynamical systems, *EPL* 99(4), 40005 (2012)

46. T. Pereira, D. Eroglu, G. B. Bagci, U. Tirnakli, and H. J. Jensen, Connectivity-driven coherence in complex networks, *Phys. Rev. Lett.* 110(23), 234103 (2013)

47. Y. Wu, J. Xiao, G. Hu, and M. Zhan, Synchronizing large number of nonidentical oscillators with small coupling, *Europhys. Lett.* 97(4), 40005 (2012)

48. X. Huang, M. Zhan, F. Li, and Z. Zheng, Single-clustering synchronization in a ring of Kuramoto oscillators, *J. Phys. A* 47(12), 125101 (2014)

49. Y. Wu, W. Liu, J. Xiao, W. Zou, and J. Kurths, Effects of spatial frequency distributions on amplitude death in an array of coupled Landau–Stuart oscillators, *Phys. Rev. E* 85(5), 056211 (2012)

50. H. Ma, W. Liu, Y. Wu, M. Zhan, and J. Xiao, Ragged oscillation death in coupled nonidentical oscillators, *Commun. Nonlinear Sci. Numer. Simul.* 19(8), 2874 (2014)

51. M. Zhan, S. Liu, and Z. He, Matching rules for collective behaviors on complex networks: Optimal configurations for vibration frequencies of networked harmonic oscillators, *PLoS ONE* 8(12), e82161 (2013)

52. H. Goldstein, C. P. Poole, and J. L. Safko, Classical Mechanics, 3rd Ed., New York: Addison-Wesley, 2002

53. D. Morin, Introduction to Classical Mechanics: With Problems and Solutions, Cambridge University Press, 2008

54. Q. Cui and I. Bahar, Normal Mode Analysis: Theory and Applications to Biological and Chemical Systems, CRC Press, 2010

55. N. W. Ashcroft and N. D. Mermin, Solid State Physics, Philadelphia: Saunders College, 1976

56. B. J. Kim, H. Hong, and M. Choi, Netons: Vibrations of complex networks, *J. Phys. Math. Gen.* 36(23), 6329 (2003)

57. E. Estrada, Universality in protein residue networks, *Biophys. J.* 98(5), 890 (2010)

58. E. Estrada, N. Hatano, and M. Benzi, The physics of communicability in complex networks, *Phys. Rep.* 514(3), 89 (2012)